Title
Squeezing Marsquakes Out of Groundwater

Journal
Geophysical Research Letters, 46(12)

ISSN
0094-8276

Authors
Manga, Michael
Zhai, Guang
Wang, Chi-Yuen

Publication Date
2019-06-28

DOI
10.1029/2019gl082892

Peer reviewed

Squeezing Marsquakes Out of Groundwater

Michael Manga[1,2], Guang Zhai[1,3], and Chi-Yuen Wang[1]

[1]Department of Earth and Planetary Science, University of California, Berkeley, Berkeley, CA, USA, [2]Center for Integrative Planetary Science, University of California, Berkeley, Berkeley, CA, USA, [3]Berkeley Seismological Laboratory, University of California, Berkeley, Berkeley, CA, USA

Correspondence to: M. Manga, manga@seismo.berkeley.edu

Abstract

Pore pressure in aquifers confined below a cryosphere will increase as Mars cools and the cryosphere thickens. Increased pore pressure decreases the effective stress and hence promotes seismicity. We calculate the rate of pore pressure change from cooling of Mars's interior and the modulation of pore pressure from solar and Phobos tides and barometric loading. Using the time-varying pressure and tidal stresses, we compute Coulomb stress changes and the expected seismicity rate from a rate-and-state friction model. Seismicity rate will vary by several tens of percent to 2 orders of magnitude if the mean pore pressure is within 0.2 and 0.01 MPa of lithostatic, respectively. Seismic events promoted by high pore pressure may be tremor-like. Documenting (or not) tidally modulated shallow seismicity would provide evidence for (or against) water-filled confined aquifers, that pore pressure is high, and that the state of stress is close to failure—with implications for processes that can deliver water to the Martian surface.

1 Introduction

Seismic signals on Mars are expected from meteorite impacts (e.g., Teanby, 2015) or may have a geodynamic origin from lithospheric stresses and ongoing mantle convection (e.g., Golombek et al., 1992; Knapmeyer et al., 2006; Panning et al., 2017; Phillips, 1991). Here we propose another internal mechanism to create marsquakes that is analogous to induced seismicity on Earth and may be modulated by tides.

Mars may host aquifers containing liquid water confined below a cryosphere (e.g., Clifford & Parker, 2001). As Mars cools, this cryosphere will thicken. If the pore space beneath the cryosphere is saturated with liquid water, the volume expansion from freezing will pressurize the remaining liquid in global or regional aquifers (e.g., Gaidos, 2001; Wang et al., 2006). As pore pressure increases, critically stressed faults are prone to slip and will thus generate marsquakes. On Earth, if the pore pressure changes are anthropogenic, the earthquakes are termed “induced”—induced seismicity is widespread where fluids are injected into the crust (Ellsworth, 2013; Zoback & Gorelick, 2012), especially from large volume injection of wastewater in Texas (e.g., Frohlich, 2012; Shirzaei et al., 2016), Oklahoma (e.g., Keranen et al., 2014), and Kansas (e.g., Schoenball & Ellsworth, 2017).

Pore pressures and crustal stresses are further modulated by solar, satellite, and barometric tides. If faults are critically stressed and close to failure, we might expect a temporal modulation of seismicity. Tides trigger deep moonquakes (e.g., Lammlein, 1977; Lognonne & Johnson, 2015). Tidal modulation of seismicity has also been documented on Earth at all types of plate boundaries, including mid-ocean ridges (e.g., Tolstoy et al., 2002), along transform boundaries (e.g., van der Elst et al., 2016), and in the form of nonvolcanic tremor in subduction zones (Rubinstein et al., 2008). Quakes caused by tides have been predicted for Europa (e.g., Hurford et al., 2018). Thus, it is not unreasonable to expect that marsquakes might also be influenced by tides, though tidal stresses will be smaller on Mars than on these other solar system bodies.

Here we compute the rate of pressure change in freezing aquifers and the modulation of that pressure from solar and Phobos tides and diurnal variations in barometric pressure. We can then compute Coulomb stress changes from tides. Using a rate-and-state friction model (Dieterich, 1994; Segall & Lu, 2015) we can predict the temporal modulation of seismicity induced in confined aquifers. We show that if background pore pressures are close to lithostatic—and hence also close to those needed to expel groundwater to the Martian surface —then there should be a tidal modulation of seismicity.

2 Pressurizing the Cryosphere

Let b be the thickness of the frozen subsurface, with surface temperature T_0 and melting temperature T_m being the temperatures and the top and bottom of this layer, respectively (Figure 1). Thermal conductivity is k. A decreasing heat flow over time t, will increase b.

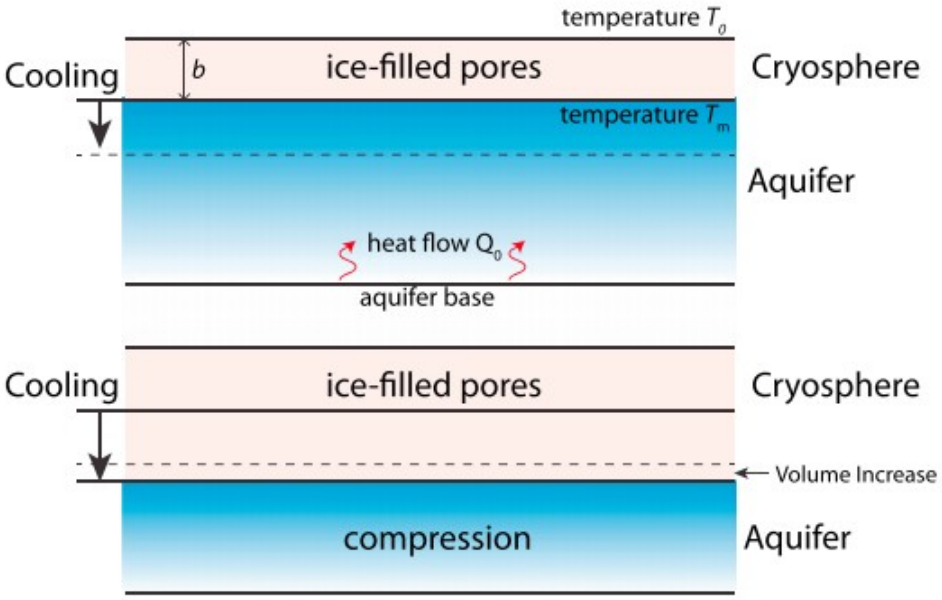

Figure 1. As Mars cools, the boundary between frozen ground and liquid water in aquifers moves downward. The volume expansion upon freezing will compress the remaining liquid water and increase pore pressure in aquifers.

To compute db/dt we rely on the decrease of heat flow obtained from numerical simulations of thermal evolution that include cooling, declining radiogenic heat production, and mantle convection. For a range of interior models and properties, present- day heat flow Q_0 is about 0.025 W/m^2 and is currently decreasing by about 0.0046 W/m^2 per Ga (Plesa et al., 2015). Parro et al. (2017) favor heat flows that are a bit lower, 0.014 to 0.025 W/m^2, with an average of 0.019 W/m^2. Uncertainties in these values are small (factor of 2) compared to uncertainties in other parameters that influence seismicity rate changes.

Neglecting any heat production within the frozen cryosphere,

$$b = k\frac{(T_m - T_0)}{Q_0} \quad (1)$$

and hence

$$\frac{\mathrm{d}b}{\mathrm{d}t} = -k\frac{(T_m - T_0)}{Q_0^2}\frac{\mathrm{d}Q_0}{\mathrm{d}t}. \quad (2)$$

Assuming a constant k=1.5 W/mK (Hartlieb et al., 2016), T_0=220 K, and T_m=273 K, then b=3,180 m and db/dt=1.85×10^{-14} m/s (equivalent to 585 m/Ga). The exact depth of the cryosphere at a given location depends on several unknowns, including the local heat flow, thermal conductivity of the crust, the salinity (composition) of the pore water (Clifford et al., 2010; Sori & Bramson, 2019), and whether or not the addition of ice to the base of the cryosphere is supply- or heat-limited (e.g., Weiss & Head, 2017). T_m could be several degrees lower than the assumed value if freezing leaves behind

sufficient salt in the aquifer (Mikucki et al., 2015). The thermal conductivity of dry, shallow regolith may be much lower and is very sensitive to the fraction of pore space filled with ice (e.g., Siegler et al., 2012).

To compute the change in pore pressure we first need to compute the change in the amount of fluid/unit volume df that arises from the 9% expansion of liquid water as it freezes. We assume that porosity ϕ decreases exponentially with depth with scale length δ,

$$\phi(z) = \phi_0 e^{-z/\delta}, \quad (3)$$

The total volume of liquid water/unit area V below the cryosphere is thus

$$V = \phi_0 \int_b^\infty e^{-z/\delta} \mathrm{d}z = \phi_0 \delta e^{-b/\delta}, \quad (4)$$

The rate that liquid water is added to V from the 9% expansion of liquid water as it freezes is $0.09\phi_0 e^{-b/\delta} \mathrm{d}b/\mathrm{d}t$. The increment of fluid content f thus varies over time

$$\frac{\mathrm{d}f}{\mathrm{d}t} = \frac{0.09\phi_0 e^{-b/\delta}}{V} \frac{\mathrm{d}b}{\mathrm{d}t}, \quad (5)$$

Choosing δ=3 km (e.g., Clifford, 1993; Hanna & Phillips, 2005) and ϕ_0=0.4 (Lewis et al., 2019), we obtain $\mathrm{d}f/\mathrm{d}t = 5.6\times10^{-19}$ s^{-1}.

The corresponding change in pore pressure p is computed using a linear poroelastic model (e.g., Wang, 2000)

$$\frac{\mathrm{d}p}{\mathrm{d}t} = \frac{K_u B}{\alpha} \frac{\mathrm{d}f}{\mathrm{d}t}, \quad (6)$$

where K_u is the undrained bulk modulus, α is the Biot-Willis coefficient, B is Skempton's coefficient, df originates from the freezing of the aquifer, and we assume this freezing is sufficiently slow that hydraulic head is uniform in the aquifer. There is much uncertainty in the relevant poroelastic properties. Here we adopt those summarized by Wang (2000) for Hanford basalt: K_u=45.4 GPa, α=0.23, and B=0.12. This leads to $\mathrm{d}p/\mathrm{d}t = 1.33\times10^{-8}$ Pa/s.

There are currently considerable uncertainties in Q_0, T_m, k, poroelastic constants, and likely lateral heterogeneities in the region (Golombek et al., 2018), which cumulatively might lead to more than an order of magnitude uncertainty in the secular stressing rate $\mathrm{d}p/\mathrm{d}t$. As we will compute, uncertainties of this magnitude in $\mathrm{d}p/\mathrm{d}t$ have a small effect on the tidal modulation of seismicity compared to other parameters. But b will affect the depth at which the seismicity would occur, and hence documenting the depth of any tidally induced seismicity should better constrain some of the poorly constrained properties of crust such as Q_0, T_m, and k. InSight measurements might also better constrain the other variables that control $\mathrm{d}p/\mathrm{d}t$.

3 Tidal Stresses and Pressure Modulation

We consider three sources of periodic deformation: changes in the gravitational potential from the Sun and Phobos, and diurnal barometric loading from atmospheric thermal tides. The geometry and equations for the time-varying strain tensor are given in the supporting information. We use degree 2 Love numbers h_2=0.29 (Genova et al., 2016; Konopliv et al., 2016) and l_2=0.038 (Sohl & Spohn, 1997), and a shear modulus of 20 GPa. We assume pure elastic deformation and neglect the lag in tidal deformation, about 0.3° for Phobos tides (e.g., Bills et al., 2005; Jacobson & Rainey, 2014).

The induced pore pressure p is

$$p = -K_u B\epsilon + B\bar{\sigma}, \quad (7)$$

where ϵ is the volumetric strain from tides (positive for expansion) and $\bar{\sigma}$ is the volumetric stress responding to the diurnal barometric loading (positive for compression). In the supporting information we describe the procedures for computing stresses and strains.

The Coulomb stress σ_c is computed from the tide-induced shear stress τ and normal stress σ_n (positive for clamping) by

$$\sigma_c = \tau - \mu(\sigma_n - \alpha p). \quad (8)$$

The friction coefficient is μ=0.6 (Byerlee, 1978).

Figure 2 shows the evolution of pore pressure and Coulomb stress at the Mars InSight lander location (4.5°N 135.9°E) for a vertical fault with a range of strikes.

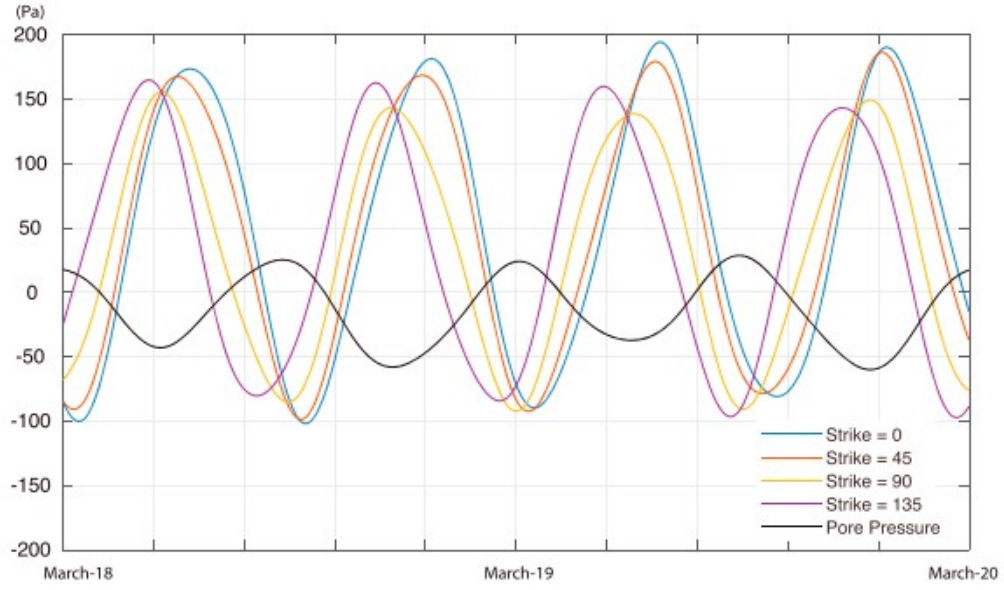

Figure 2. Time series of Coulomb stress change for different fault azimuths (vertical faults) and pore pressure change due to the combined effect of solar and Phobos tides and barometric loading. We assume the location of the InSight lander. Dates are Earth dates in 2019.

The magnitudes of the tidal stresses and pore pressure changes are small (of order 10^2 Pa). However, the tidal stressing rate is several orders of magnitude larger than the secular rate of pressurization from freezing aquifers. If the shallow crust is critically stressed by the long-term thermal contraction (e.g., Knapmeyer et al., 2006), mantle convection (Plesa et al., 2016), or freezing of aquifers (section 2), then faults near failure may be ubiquitous and the tidal stresses and pore pressures may trigger earthquakes on critically stressed faults. The relatively large magnitude of tidal forcing may control the timing of seismicity.

4 Predicting Seismicity Rate on Mars

To predict seismic activity on Mars, we use a laboratory-derived rate-and-state earthquake nucleation model (Dieterich, 1994). This model simulates the temporal evolution of seismicity rate due to a change of Coulomb failure stress and assumes that fault systems are critically stressed. A simplified version of the nucleation model (Segall & Lu, 2015) relates the history of relative seismicity rate R (seismicity rate relative to background seismicity rate) to the history of Coulomb stressing rate

$$\frac{\mathrm{d}R}{\mathrm{d}t} = \frac{R}{t_a}\left(\frac{\dot{\sigma}_c}{\dot{\tau}_0} - R\right) \quad (9)$$

where $\dot{\tau}_0$ is the background stressing rate from Mars's secular cryosphere cooling, which is the lower bound and may be as much as 2 orders of magnitudes larger, as summarized in Panning et al. (2017); $t_a = A\sigma_0/\dot{\tau}_0$ is the characteristic relaxation time; A is a constitutive parameter in the rate-and-state friction law (Dieterich, 1994); σ_0 is the background effective normal stress that depends on the absolute pore fluid pressure in the aquifers. The Coulomb stressing rate $\dot{\sigma}_c$ is calculated from equation 8 by superimposing the tidal and barometric loading induced pore pressure history p and the Coulomb stress without pore pressure (Figure 2). We use the value of A=0.003 from Segall and Lu (2015) and highlight that its value and uncertainty are unknown for Mars. Values and uncertainties in A, σ_0, and $\dot{\tau}_0$ affect t_a; hence, we explore a range of t_a.

Using the stressing history (Figure 2), we can predict the temporal evolution of seismicity rate on Mars by integrating equation 9. Figure 3 shows that background effective normal stress σ_0 dominates the predicted seismicity rate changes from tidal and barometric effects. Parameters that affect b and db/dt and hence the background stressing rates have a relatively small effect because they are always much smaller than those produced by tides unless the effective normal stress is low. If the background normal stress is high, the fault system would be relatively stable to small stress fluctuations, making marsquakes difficult to nucleate (Figure 3, top row). However, if the pore fluid pressure is close to lithostatic pressure such that the effective normal stress would be small, the fault system is sensitive to small stress fluctuations and the relative seismicity rate can approach 10^3 (Figure 3,

bottom row). The nonlinearity of rate-and-state friction further influences the seismicity rate as the effective normal stress becomes small. The increase in the number of marsquakes can also elevate marsquake magnitude by more than 2 orders following the Gutenberg-Richter earthquake magnitude-frequency relationship.

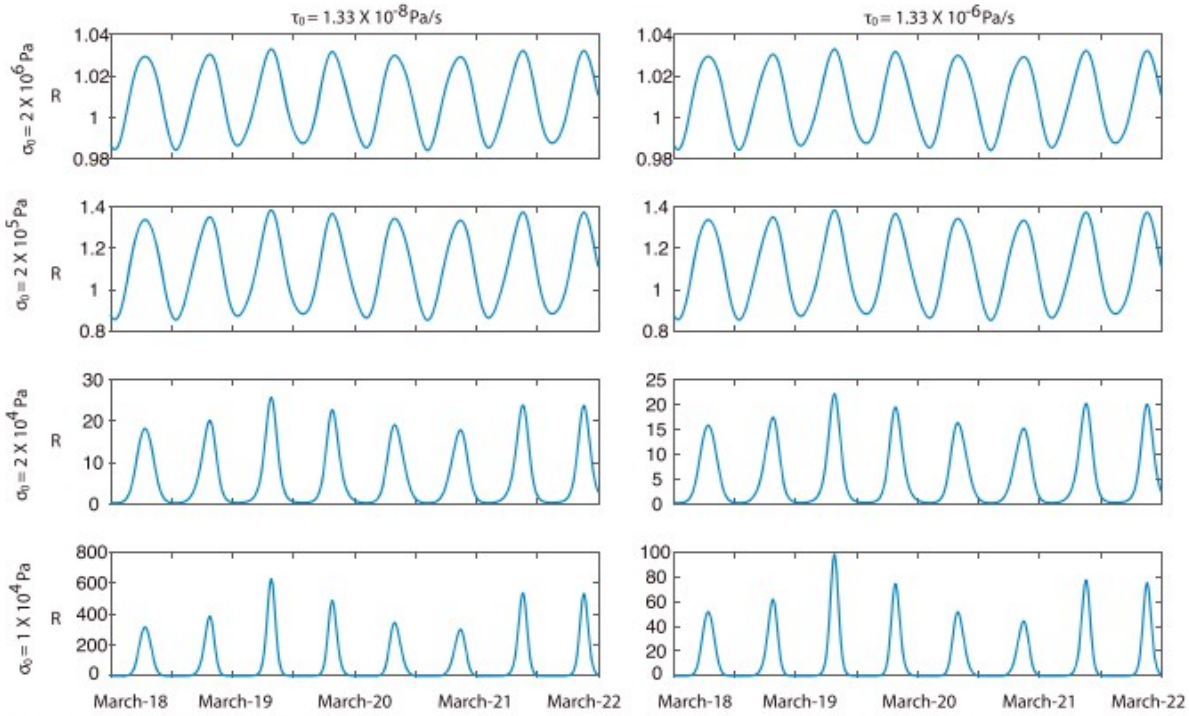

Figure 3. The simulated time series of relative seismicity rate R due to imparted stresses and pore pressure changes assuming $A = 0.003$ (Segall and Lu, 2015) for different scenarios of background effective normal stress σ_0 and background stressing rate $\dot{\tau}_0$ (lower limit (left column) is the stressing rate from freezing the cryosphere and the larger value (right column) is 100 times larger). We consider σ_0 as large as 2 MPa (top row). We consider a lower value of σ_0 (bottom row) by choosing a lower bound of 0.5% of the largest σ_0. Dates are Earth dates in 2019.

Figure 3 shows how the seismicity rate R is expected to vary. We do not, at the present time, convert the seismicity rate to a prediction of Mars's total marsquake magnitude-time distribution, which could be compared with data from InSight. To do so requires three additional steps, in addition to knowing the background seismicity rate: (1) integrating R over the surface of Mars, (2) accounting for attenuation and scattering in the shallow crust, and (3) modeling the noise environment produced from thermal effects and wind which will vary throughout the Martian day and over seasons. InSight should provide much of the data needed to do this calculation.

Since Mars's orbit has large eccentricity that causes the gravitational attraction of the Sun to change by a factor of 1.74 per orbit, we expect a further modulation of marsquakes throughout the year (supporting information Figure S3). Identifying variations in seismicity from semidiurnal to annual timescales may help distinguish the origin of the stress connected

to marsquakes and hence provide an opportunity to identify groundwater-induced seismicity.

5 Discussion

The physics used to compute whether tidal stresses and freezing aquifers influence seismicity are similar to those used to forecast induced seismicity on Earth (e.g., Goebel & Brodsky, 2018; Zhai & Shirzaei, 2018). There are, however, many poroelastic and aquifer properties (K_u, B, α, ϕ_0, δ) that are not observationally constrained on Mars, and statistical properties of seismicity that enter the rate-and-state friction model (A, $\dot{\tau}_0$) are not known. As a consequence, there are corresponding uncertainties in the mean seismicity rate and its modulation. The parameter, however, that is most uncertain and has the largest effect on the magnitude of R is σ_0, the background effective normal stress (that depends on the mean pore fluid pressure in the aquifers) as it leads to a rapid change in seismicity rate as pore pressure approaches lithostatic. Uncertainties in the parameters that control b primarily affect the depth at which any tidally modulated seismicity would occur. Thus, the general conclusion that tidal modulation is expected if pore pressure is close to lithostatic should be a robust conclusion.

Identifying any tidal modulation of shallow seismicity could then be used to better constrain properties of the Martian crust and any aquifers it hosts, at least in the vicinity of the InSight landing site (Golombek et al., 2018)—seismicity enabled by high pore pressure is expected to occur near the base of the cryosphere. Tidally induced seismicity might also be tremor-like, similar to nonvolcanic tremor on Earth that is often attributed to high pore pressures (e.g., Beroza & Ide, 2011). The first reported marsquake on sol 128 (reported by the InSight team on 23 April 2019) does in fact look tremor-like, but this type of waveform could also be the result of multiple scattering in the crust.

We have drawn an analogy of the hypothesized tidallymodulated seismicity to induced seismicity on Earth because high fluid pressures promote slip and pressure variations modify the timing of seismic events. There is, however, a quantitative difference because the pore pressure changes from tidally induced strains are relatively small compared to the shear stresses—the relative magnitude of pressure and shear stress changes from tides are small compared to the equivalent from fluid injection. Tidal modulation of seismicity does not necessitate high fluid pressure change—deep moonquakes provide a counter example—but does require small effective normal stresses.

The outflow channels on Mars are usually attributed to the catastrophic release of groundwater from the Martian subsurface (e.g., Carr, 1979). Discharge from present-day aquifers has also been suggested as a mechanism to form smaller features such as gullies and recurring slope linea (e.g., Heldmann et al., 2005; Malin & Edgett, 2000; Mellon & Phillips, 2001; Stillman et al., 2014), possibly enabled because high salinity can decrease

the depth at which aquifers remain stable (Ojha et al., 2015; Stillman et al., 2016). Yet the source of the water and the mechanism by which the water is released remain uncertain (e.g., Clifford & Parker, 2001; Grimm et al., 2017; Hanna & Phillips, 2005, 2006; Wang et al., 2005). Freezing of aquifers may allow pore pressure to approach lithostatic pressure at the base of the cryosphere and hence to rupture the cryosphere, leading to groundwater discharge on the Martian surface (e.g., Gaidos, 2001; Wang et al., 2006). It remains uncertain, however, whether pressurization of Martian aquifers by gradual freezing can create sufficiently high pore pressure to rupture the cryosphere (Hanna & Phillips, 2005), though water loss has been low enough that groundwater should at least persist globally (Grimm et al., 2017). Pressure in aquifers confined by a cryosphere may also be elevated if they are recharged at higher elevation (e.g., Andrews-Hanna & Lewis, 2011; Harrison & Grimm, 2004).

The ideas and processes considered here for Mars may not be confined to rocky planets with groundwater systems (Earth and Mars). Fracturing by overpressure that develops in water confined by a freezing ice shell has also been invoked for icy satellites, for water confined both in a global ocean (e.g., Manga & Wang, 2007) and possibly in isolated pockets of water (e.g., Fagents, 2003; Manga & Michaut, 2017).

6 Summary

Shallow, tidally modulated seismicity, if documented by InSight or the accelerometer on Curiosity (Lewis et al., 2019), would provide evidence of liquid-filled confined aquifers with near-lithostatic pore pressure and a state of stress close to that required for failure. Conversely, an absence of tidal modulation of seismicity implies low pore pressure, with implications for the properties of Martian groundwater systems and the processes that allow liquid water to be delivered to the Martian surface. Constraining the depth of Mars's cryosphere and whether it is underlain by liquid water are critical to understanding Mars's past and present near-surface water budget (Carr & Head, 2015). The presence or absence of induced seismicity provides an opportunity to better constrain the state and amount of subsurface water.

Acknowledgments

M. M. is supported by NASA 80NSSC19K0545, C. W. by NSF 1463997 and G. Z. by DOE DE-SC0019307. We thank the entire InSight team for their persistence and dedication to a most remarkable geophysical achievement, and the Editor, M. Panning, and an anonymous reviewer for constructive and thoughtful comments. No data was presented in this paper. Curves in Figures 2 and 3 are produced by solving the equations in the paper.

References

Andrews-Hanna, J. C., & Lewis, K. W. (2011). Early Mars hydrology: 2. Hydrological evolution in the Noachian and Hesperian epochs. *Journal of Geophysical Research*, 116, E02007. https://doi.org/10.1029/2010JE003709

Beroza, G. C., & Ide, S. (2011). Slow earthquakes and nonvolcanic tremor. *Annual Reviews of Earth and Planetary Sciences*, 39, 271– 296. https://doi.org/10.1146/annurev-earth-040809-152531

Bills, B. G., Neumann, G. A., Smith, D. E., & Zuber, M. T. (2005). Improved estimate of tidal dissipation within Mars from MOLA observations of the shadow of Phobos. *Journal of Geophysical Research*, 110, E07004. https://doi.org/10.1029/2004JE002376

Byerlee, J. (1978). Friction of Rocks. *Pure and Applied Geophysics*, 116, 615– 626.

Carr, M. H. (1979). Formation of Martian flood features by release of water from confined aquifers. *Journal of Geophysical Research*, 87, 6781– 6790.

Google ScholarUC-eLinks

Carr, M. H., & Head, J. W. (2015). Martian surface/near-surface water inventory: Sources, sinks, and changes with time. *Geophysical Research Letters*, 42, 726– 732. https://doi.org/10.1002/2014GL062464

Clifford, S. M. (1993). A model for the hydrologic and climatic behavior of water on Mars. *Journal of Geophysical Research*, 98, 10,973– 11,016.

Clifford, S. M., Lasue, J., Heggy, E., Boisson, J., McGovern, P., & Max, M. D. (2010). Depth of the Martian cryosphere: Revised estimates and implications for the existence and detection of subpermafrost groundwater. *Journal of Geophysical Research*, 115, E07001. https://doi.org/10.1029/2009JE003462

Clifford, S. M., & Parker, T. J. (2001). The evolution of the Martian hydrosphere: Implications for the fate of a primordial ocean and the current state of the Northern Plains. *Icarus*, 154, 40– 79.

Dieterich, J. (1994). A constitutive law for rate of earthquake production and its application to earthquake clustering. *Journal of Geophysical Research*, 99(B2), 2601– 2618.

Ellsworth, W. L. (2013). Injection-induced earthquakes. *Science*, 341(6142), 1225942. https://doi.org/10.1126/science.1225942

Fagents, S. A. (2003). Considerations for effusive cryovolcanism on Europa: The post-Galileo perspective. *Journal of Geophysical Research*, 108(E12), 5139. https://doi.org/10.1029/2003JE002128

Frohlich, C. (2012). Two-year survey comparing earthquake activity and injection-well locations in the Barnett Shale, Texas. *Proceedings of the National Academy of Sciences*, 109(35), 13,934– 13,938.

Gaidos, E. J. (2001). Cryovolcanism and the recent flow of liquid water on Mars. *Icarus*, 153(1), 218– 223.

Genova, A., Goosens, S., Lemoine, F. G., Mazarico, E., Neumann, G. A., Smith, D., & Zuber, M. T. (2016). Seasonal and static gravity field of Mars from MGS, Mars Odyssey and MRO radio science. *Icarus*, 272, 228– 245. https://doi.org/10.1016/j.icarus.2016.02.050

Goebel, T. H., & Brodsky, E. E. (2018). The spatial footprint of injection wells in a global compilation of induced earthquake sequences. *Science*, 361(6405), 899– 904.

Golombek, M., Banerdt, W., Tanaka, K., & Tralli, D. (1992). A prediction of Mars seismicity from surface faulting. *Science*, 258, 979– 981.

Golombek, M., Grott, M., Kargl, G., Andrade, J., Marshall, J., Warner, N., Teanby, N. A., Ansan, V., Hauber, E., Voigt, J., Lichtenheldt, R., Knapmeyer-Endrun, B., Daubar, I. J., Kipp, D., Muller, N., Lognonné, P., Schmelzbach, C., Banfield, D., Trebi-Ollennu, A., Maki, J., Kedar, S., Mimoun, D., Murdoch, N., Piqueux, S., Delage, P., Pike, W. T., Charalambous, C., Lorenz, R., Fayon, L., Lucas, A., Rodriguez, S., Morgan, P., Spiga, A., Panning, M., Spohn, T., Smrekar, S., Gudkova, T., Garcia, R., Giardini, D., Christensen, U., Nicollier, T., Sollberger, D., Robertsson, J., Ali, K., Kenda, B., & Banerdt, W. B. (2018). Geology and physical properties investigations by the InSight Lander. *Space Science Reviews*, 214, 84. https://doi.org/10.1007/s11214-018-0512-7

Grimm, R. E., Harrison, K. P., Stillman, D. E., & Kirchoff, M. R. (2017). On the secular retention of ground water and ice on Mars. *Journal of Geophysical Research: Planets*, 122, 94– 109. https://doi.org/10.1002/2016JE005132

Hanna, J. C., & Phillips, R. J. (2005). Hydrological modeling of the Martian crust with application to the pressurization of aquifers. *Journal of Geophysical Research*, 110, E01004. https://doi.org/10.1029/2004JE002330

Hanna, J. C., & Phillips, R. J. (2006). Tectonic pressurization of aquifers in the formation of Mangala and Athabasca Valles, Mars. *Journal of Geophysical Research*, 111, E03003. https://doi.org/10.1029/2005JE002546

Harrison, K. P., & Grimm, R. E. (2004). Tharsis recharge: A source of groundwater for Martian outflow channels. *Geophysical Research Letters*, 31, L14703. https://doi.org/10.1029/2004GL020502

Hartlieb, P., Toifl, M., Kuchar, F., Meisels, R., & Antretter, T. (2016). Thermo-physical properties of selected hard rocks and their relation to microwave-assisted comminution. *Minerals Engineering*, 91, 34– 41.

Heldmann, J. L., Toon, O. B., Pollard, W. H., Mellon, M. T., Pitlick, J., McKay, C. P., & Andersen, D. T. (2005). Formation of Martian gullies by the action of liquid water flowing under current Martian environmental conditions. *Journal of Geophysical Research*, 110, E05004. https://doi.org/10.1029/2004JE002261

Hurford, T. A., Henning, W. G., Maguire, R., Lekic, V., Schmerr, N., Panning, M., Bray, V. J., Manga, M., Kattenhorn, S. A., Quick, L. C., & Rhoden, A.

R. (2018). Seismicity on tidally active solid-surface worlds. arXiv preprint arXiv:1811.06536.

Jacobson, R. A., & Rainey, V. (2014). Martian satellite orbits and ephemerides. *Planetary and Space Science*, 102, 35– 44.

Keranen, K., Weingarten, M., Abers, G., Bekins, B., & Ge, S. (2014). Sharp increase in central Oklahoma seismicity since 2008 induced by massive wastewater injection. *Science*, 345(6195), 448– 451.

Knapmeyer, M., Oberst, J., Hauber, E., Wahlisch, M., Deuchler, C., & Wagner, R. (2006). Working models for spatial distribution and level of Mars' seismicity. *Journal of Geophysical Research*, 111, E11006. https://doi.org/10.1029/2006JE002708

Konopliv, A. S, Park, R. S., & Folkner, W. M. (2016). An improved JPL Mars gravity field and orientation from Mars orbiter and Lander tracking data. *Icarus*, 274, 253– 260. https://doi.org/10.1016/j.icarus.2016.02.052

Lammlein, D. R. (1977). Lunar seismicity and tectonics. *Physics of the Earth and Planetary Interiors*, 14(3), 224– 273.

Lewis, K. W., Peters, S., Gonter, K., Morrison, S., Schmerr, N., Vasavada, A. R., & Gabriel, T. (2019). A surface gravity traverse on Mars indicates low bedrock density at Gale crater. *Science*, 363, 535– 537.

Lognonne, P., & Johnson, C. L. (2015). Planetary seismology (2nd ed.). In G. Schubert (Ed.), *Treatise on Geophysics* (Vol. 10, pp. 65– 120). Oxford: Elsevier.

Malin, M. C., & Edgett, K. S. (2000). Evidence for recent groundwater seepage and surface runoff on Mars. *Science*, 288(5475), 2330– 2335.

Manga, M., & Michaut, C. (2017). Formation of lenticulae on Europa by saucer-shaped sills. *Icarus*, 286, 261– 269. https://doi.org/10.1016/j.icarus.2016.1009

Manga, M., & Wang, C.-Y. (2007). Pressurized oceans and the eruption of liquid water on Europa and Enceladus. *Geophysical Research Letters*, 34, L07202. https://doi.org/10.1029/2007GL029297

Mellon, M. T., & Phillips, R. J. (2001). Recent gullies on Mars and the source of liquid water. *Journal of Geophysical Research*, 106(E10), 23,165– 23,179.

Mikucki, J. A., Auken, E., Tulaczyk, S., Virginia, R. A., Schamper, C., Sørensen, K. I., Doran, P. T., Dugan, H., & Foley, N. (2015). Deep groundwater and potential subsurface habitats beneath an Antarctic dry valley. *Nature Communications*, 6, 6831. https://doi.org/10.1038/ncomms7831

Ojha, L., Wilhelm, M. B., Murchie, S. L., McEwen, A. S., Wray, J. J., Hanley, J., Massé, M., & Chojnacki, M. (2015). Spectral evidence for hydrated salts in recurring slope lineae on Mars. *Nature Geoscience*, 8(11), 829– 832.

Panning, M. P., Lognonné, P., Banerdt, W. B., Garcia, R., Golombek, M., Kedar, S., Knapmeyer-Endrun, B., Mocquet, A., Teanby, N. A., Tromp, J., Weber, R., Beucler, E., Blanchette-Guertin, J.-F., Bozdag, E., Drilleau, M., Gudkova, T., Hempel, S., Khan, A., Lekic, V., Murdoch, N., Plesa, A.-C., Rivoldini, A., Schmerr, N., Ruan, Y., Verhoeven, O., Gao, C., Christensen, U., Clinton, J., Dehant, V., Giardini, D., Mimoun, D., Thomas Pike, W., Smrekar, S., Wieczorek, M., Knapmeyer, M., & Wookey, J. (2017). Planned products of the Mars structure service for the InSight mission to Mars. *Space Science Reviews*, 211(1-4), 611– 650.

Parro, L. M., Jiménez-Díaz, A., Mansilla, F., & Ruiz, J. (2017). Present-day heat flow model of Mars. *Scientific Reports*, 7, 45629. https://doi.org/10.1038/srep45629

Phillips, R. (1991). Expected rate of Marsquakes, in scientifc rationale and requirements for a global seismic network on Mars (LPI Tech. Rept., 91-02, pp. 35– 38). Houston: Lunar and Planetary Inst.

Plesa, A. C., Grott, M., Tosi, N., Breuer, D., Spohn, T., & Wieczorek, M. A. (2016). How large are present-day heat flux variations across the surface of Mars? *Journal of Geophysical Research: Planets*, 121, 2386– 2403. https://doi.org/10.1002/2016JE005126

Plesa, A. C., Tosi, N., Grott, M., & Breuer, D. (2015). Thermal evolution and Urey ratio of Mars. *Journal of Geophysical Research: Planets*, 120, 995– 1010. https://doi.org/10.1002/2014JE004748

Rubinstein, J. L., La Rocca, M., Vidale, J. E., Creager, K. C., & Wech, A. G. (2008). Tidal modulation of nonvolcanic tremor. *Science*, 319(5860), 186– 189.

Schoenball, M., & Ellsworth, W. L. (2017). A systematic assessment of the spatiotemporal evolution of fault activation through induced seismicity in Oklahoma and southern Kansas. *Journal of Geophysical Research: Solid Earth*, 122, 10,189– 10,206. https://doi.org/10.1002/2017JB014850

Segall, P., & Lu, S. (2015). Injection-induced seismicity: Poroelastic and earthquake nucleation effects. *Journal of Geophysical Research: Solid Earth*, 120, 5082– 5103. https://doi.org/10.1002/2015JB012060

Shirzaei, M., Ellsworth, W. L., Tiampo, K. F., González, P. J., & Manga, M. (2016). Surface uplift and time-dependent seismic hazard due to fluid injection in eastern Texas. *Science*, 353(6306), 1416– 1419. https://doi.org/10.1126/science.aag0262

Siegler, M., Aharonson, O., Carey, E., Choukroun, M., Hudson, T., Schorghofer, N., & Xu, S. (2012). Measurements of thermal properties of icy Mars regolith analogs. *Journal of Geophysical Research*, 117, E03001. https://doi.org/10.1029/2011JE003938

Sohl, F., & Spohn, T. (1997). The interior structure of Mars: Implications from SNC meteorites. *Journal of Geophysical Research*, 102, 1613– 1635.

Sori, M. M., & Bramson, A. M. (2019). Water on Mars, with a grain of salt: Local heat anomalies are required for basal melting of ice at the South Pole today. *Geophysical Research Letters*, 46, 1222– 1231. https://doi.org/10.1029/2018GL080985

Stillman, D. E., Michaels, T. I., Grimm, R. E., & Hanley, J. (2016). Observations and modeling of northern mid-latitude recurring slope lineae (RSL) suggest recharge by a present-day Martian briny aquifer. *Icarus*, 265, 125– 138. https://doi.org/10.1016/j.icarus.2015.10.007

Stillman, D. E., Michaels, T. I., Grimm, R. E., & Harrison, K. P. (2014). New observations of Martian southern mid-latitude recurring slope lineae (RSL) imply formation by freshwater subsurface flows. *Icarus*, 233, 328– 341. https://doi.org/10.1016/j.icarus.2014.01.017

Teanby, N. A. (2015). Predicted detection rates of regional-scale meteorite impacts on Mars with the InSight shortperiod seismometer. *Icarus*, 256, 49– 62.

Tolstoy, M., Vernon, F. L., Orcutt, J. A., & Wyatt, F. K. (2002). Breathing of the seafloor: Tidal correlations of seismicity at Axial volcano. *Geology*, 30(6), 503– 506.

van der Elst, N. J., Delorey, A. A., Shelly, D. R., & Johnson, P. A. (2016). Fortnightly modulation of San Andreas tremor and low-frequency earthquakes. *Proceedings of the National Academy of Sciences*, 113(31), 8601– 8605.

Wang, H. (2000). *Theory of linear poroelasticity with applications to geomechanics and hydrogeology*. Princeton, NJ: Princeton University Press.

Wang, C. Y., Manga, M., & Hanna, J. C. (2006). Can freezing cause floods on Mars? *Geophysical Research Letters*, 33, L20202. https://doi.org/10.1029/2006GL027471

Wang, C.-Y., Manga, M., & Wong, A. (2005). Floods on Mars released from groundwater by impact. *Icarus*, 175, 551– 555.

Weiss, D. K., & Head, J. W. (2017). Evidence for stabilization of the ice-cemented cryosphere in earlier Martian history: Implications for the current abundance of groundwater at depth on Mars. *Icarus*, 288, 120– 147.

Zhai, G., & Shirzaei, M. (2018). Fluid injection and time-dependent seismic hazard in the Barnett Shale, Texas. *Geophysical Research Letters*, 45, 4743– 4753. https://doi.org/10.1029/2018GL077696

Zoback, M. D., & Gorelick, S. M. (2012). Earthquake triggering and large-scale geologic storage of carbon dioxide. *Proceedings of the National Academy of Sciences*, 109(26), 10,164– 10,168.